Agricultural and Forest Meteorology 334 (2023) 109436

Contents lists available at ScienceDirect

Agricultural and Forest Meteorology

journal homepage: www.elsevier.com/locate/agrformet

Experiments and COMSOL simulations: A comparative study of the heat flux plate method and the gradient method for soil heat flux measurements in barren sand

Tianyue Zhao [a], Zhaoyu Qiao [a], Yuanyuan Zhang [a], Binxiang Huang [b], Robert Horton [c], Gang Liu [a,*]

[a] Department of Land Use Engineering, College of Land Science and Technology, China Agricultural University, Beijing 100193, China
[b] College of Resources and Environmental Sciences, China Agricultural University, Beijing, 100193, China
[c] Department of Agronomy, Iowa State Univ., Ames, IA 50011, United States of America

ARTICLE INFO

Keywords:
Heat flux plate
Gradient method
Soil heat flux
Finite element simulation
Thermo-TDR
Heat pulse method

ABSTRACT

Soil heat flux (G) is important for studying the energy balance at the soil-atmosphere interface. In most cases, a reference flux (true value) is not available for soil heat flux. The heat flux plate method and the heat pulse sensor gradient method are two commonly used methods to measure soil heat flux. Both methods have inherent shortcomings that lead to unavoidable measurement errors. There is a need for a theoretical analysis to identify the origin of errors associated with the gradient method. In this study, by introducing a plane heater of known heating strength to generate a one-dimensional heat flux, we compared the measurements of soil heat flux by both methods at different soil moisture contents for laboratory (indoor) and field (outdoor) experiments, as well as computer simulations for a sandy soil. Differences between the COMSOL simulation results and the indoor measurements were less than 15%, indicating that the COMSOL simulated soil heat flux results were reliable. The indoor experiments provided close agreement between the heat flux plate method and the gradient method (Pearson's correlation coefficient $r \geq 0.993$). The results of the field experiments showed that the correlation coefficient of the two methods decreased by at least 9.3%. Our field measurements indicated that the gradient method is not suitable for measuring G in the presence of alternating freezing-thawing soil conditions. Although heat flux plates have several short-comings, they may perform better than the heat pulse sensor gradient method in partially frozen soils. The finite difference approximation of nonlinear thermal gradients causes errors in the gradient method heat flux values. However, this gradient method error could be eliminated by altering the heat pulse probe positioning with depth to provide finer scale measurements of temperature with depth.

1. Introduction

Surface energy balance is an important area of research in agriculture, forestry, meteorology and ecology (Mauder et al., 2020). Soil heat flux (G) is a particularly important component of the surface energy balance of bare soils (Choudhury et al., 1987; Idso et al., 1975), areas without dense vegetation, and forests. Difficulties in energy balance closure have been reported, i.e., the sum of net radiation and surface heat fluxes is found to be greater than the sum of turbulent fluxes in several cases (Foken et al., 1995; Foken, 2008; Wilson et al., 2002). Errors in G measurements as well as errors in soil heat storage (Leuning et al., 2012) are two factors that warrant further consideration.

Two common methods to measure G are the soil heat flux plate method (Sauer, 2002) and the gradient method (Cobos and Baker, 2003). Although, Peng et al. (2015) chose the values of the gradient method as a standard, the validation of their choice requires further testing. In addition, for most experiments, a known reference value of G is not available (Russell et al., 2015). As a result, there is uncertainty on the accuracies of the heat flux plate and gradient methods (Wu et al., 2020). For example, without verification and lacking a reference G, Peng et al. (2015) assume that the gradient method is more accurate than the heat flux plate method. Although there are experiments designed to evaluate the performance of various kinds of heat flux plates with a reference G value, most of the experiments were performed under

* Corresponding author.
E-mail address: liug@cau.edu.cn (G. Liu).

https://doi.org/10.1016/j.agrformet.2023.109436
Received 31 August 2022; Received in revised form 18 February 2023; Accepted 20 March 2023
Available online 28 March 2023

steady state conditions (Sauer et al., 2007, 2008; van Loon et al., 1998; Watts et al., 1990). To our knowledge, there are few transient experiments (Fuchs and Tanner, 1968; Howell and Tolk, 1990) that use known reference G values (by using a plane heater to set soil heat fluxes to some given values), and no research has evaluated the accuracy of the heat flux plate method and the gradient method simultaneously with a known reference G (true value of G).

Although the heat flux plate method is more popular than the gradient method for measuring G (Mayocchi and Bristow, 1995; van Loon et al., 1998; Watts et al., 1990), some assert the gradient method is superior to the heat flux plate method (Lu et al., 2016; Peng et al., 2015), mainly because heat flux plates alter the natural soil environment by disrupting liquid and vapor movement. To our knowledge, few studies have explored the potential errors in G measurements with the gradient method. There are several sources of error when using a dual needle heat pulse (DPHP) probe measurements to make gradient method determinations. First, the DPHP sensor probe spacing is prone to change over time which compromises the performance. The theoretical analysis of Liu et al. (2008) demonstrated that, for both heating and temperature probes of DPHP method, 1° deflections of the probes, led to > 10% errors in thermal conductivity and heat capacity. In addition, the thermal contact resistance (Liu et al., 2017) between the soil and the DPHP needle can lead to an overestimation of the dry soil specific heat (c) by at least 20% (Liu et al., 2012; Ren et al., 1999). Wind above the surface (Sang et al., 2020, 2021), and spatial heterogeneity can lead to errors in thermal property measurements. The influence of thermal property measurement errors on the accuracy of G measurements will be discussed and analyzed extensively in this paper.

In addition to measurements, numerical simulations (Faucher-Giguère et al., 2008) provide a means to evaluate the performance of the gradient method and heat flux plates. Finite element simulations have been used to study DPHP probes (Liu et al., 2013, 2016; Sang et al., 2020). Numerical simulations (e.g., COMSOL, Hydrus) have advantages that cannot be matched by physical experiments. Unlike physical experiments which are limited to a few points of measurement, numerical software can simulate a temperature field or fluid field with spatial distributions of various physical parameters. In addition, simulations avoid the effects of various unknown factors in field tests, such as soil spatial heterogeneity (Wu et al., 2020), inhomogeneity of the temperature field (Jury and Bellantuoni, 1976), and stochastic surface wind speeds (Sang et al., 2020). Unlike traditional experiments (heat flux plate measurements and gradient method measurements) which are time consuming and labor intensive, computer simulations are fast and accurate. To the best of our knowledge, few COMSOL simulations have been used to simulate soil heat flux plates and the gradient method.

In this study, our objectives are to: (1) Use a plane heater film with a specific heating strength and use COMSOL simulations to test the hypothesis of Peng et al. (2015) that the gradient method provides standard values of G. (2) Evaluate the measurement errors of the heat flux plate method and the gradient method under indoor and outdoor conditions. (3) Examine the feasibility of using COMSOL simulations of G to evaluate the performance of several commonly used soil heat flux plates.

2. Materials and methods

2.1. Theoretical G expression and philip's correction equation

We derived a theoretical G value based on an analytical solution of heat conduction. In this way, we can use the analytical value of G as the reference to evaluate the performances of the gradient method and the heat flux plate method. In a semi-infinite soil with zero initial temperature, denoting the heat flux at $z = 0$ cm as F_0 (W m^{-2}), then

$$G(0,t) = F_0 \tag{1}$$

This heat flow will cause the following temperature, T, distribution as a function of depth, z, and time, t (Eq. (7) of Carslaw and Jaeger (1959: p75)

$$T(z,t) = \frac{2F_0}{\lambda}\left[\left(\frac{\alpha t}{\pi}\right)^{\frac{1}{2}} e^{-\frac{z^2}{4\alpha t}} - \frac{z}{2} erfc\frac{z}{2\sqrt{\alpha t}}\right] \tag{2}$$

where α (m^2 s^{-1}) is the soil thermal diffusivity, λ (W m^{-1} K^{-1}) is the soil thermal conductivity. The soil heat flux as a function of depth and time is (Eq. (4) of Carslaw and Jaeger (1959: p75))

$$G(z,t) = F_0 erfc\frac{z}{2\sqrt{\alpha t}} \tag{3}$$

Here, $erfc(x)$ is the error function. For a specific heat flux density F_0 at $z = 0$ cm, Eq. (3) gives the theoretical value of the soil heat flux at depth z, which will used as the reference value of G for specific indoor experiments.

In order to reduce measurement errors due to temperature field distortions near a heat flux plate (Sauer et al., 2003; Watts et al., 1990), the correction formula of Philip (1961) was applied. By approximating the heat flux plate as an ellipsoid, Philip (1961) derived the heat flux correction parameter (f)

$$f = \frac{\in}{1 + (\in -1)H} \tag{4}$$

where $\in$ is the ratio of the thermal conductivity of the heat flux plate to the thermal conductivity of the soil, and H is a shape factor which depends on the geometric characteristics of the heat flux plate (diameter, width, thickness, etc.). For a thin circular plate with diameter a and thickness b, H satisfies

$$H = 1 - 1.92\frac{b}{a} \tag{5}$$

Soil heat flux after applying Philip's correction method is

$$G_{philp} = G/f \tag{6}$$

2.2. Indoor experiments

For laboratory (indoor) experiments, we used a sandy soil (98.2% sand, 1.7% silt, 0.1% clay). The specific heat of the sandy soil measured by a differential scanning calorimetry (Q2000 DSC, TA Instruments, New Castle, DE) is 751 J kg^{-1} K^{-1}. The bulk density (ρ) of the sandy soil for the indoor experiments was 1650 kg m^{-3}. We mixed dry soil and distilled water to establish three soil water contents, 0 g g^{-1}, 0.02 g g^{-1} and 0.15 g g^{-1}. To ensure uniform spatial distributions of soil water, moistened samples were sealed in plastic bags for 48 h and then packed into cylindrical Plexiglas containers (12 cm diameter and 10 cm height). Each container had a lid to prevent evaporation. Soil thermal conductivity (λ) and specific heat capacity (c) were measured in each packed container with a DPHP probe. The results are shown in Table 1.

By using soil thermal conductivity values computed a from theoretical model, Kimball et al. (1976) demonstrated that when used properly, the gradient method can provide reliable surface soil-heat flux values. A DPHP sensor has been used to measure soil heat flux with the gradient method (Ochsner et al., 2006; Heitman et al., 2008; Peng et al., 2015). The gradient method is based on Fourier's law $G = -\lambda \nabla T$ (Kimball et al., 1976; Heitman et al., 2008), G is calculated approximately as:

Table. 1
Measured sandy soil thermal conductivity, λ, and specific heat capacity at various water contents.

Water content	λ	Specific heat capacity
g g^{-1}	W m^{-1} K^{-1}	J kg^{-1} K^{-1}
0	0.30±0.01	751±2
0.02	0.80±0.01	803±8
0.15	1.46±0.05	1175±15

$$G \approx -\lambda \frac{\Delta T}{\Delta z} \tag{7}$$

Detailed information on the procedure to calculate G (Eq. (7)) based on the gradient method is given by Heitman et al. (2008). The gradient method has several advantages over the heat flux plate method, including less soil disturbance during installation (Heitman et al., 2008), less blockage to infiltrating water, and less blockage to vapor movement (Heitman et al., 2008). Eq. (7) is most accurate when the spatial resolution of the probe is small, i.e. $\Delta z \to 0$. According to Fourier's law and the Taylor expansion for analytical functions (Thomas et al., 2014), using Eq. (7) will have a truncation error. In the results and discussion section, we will illustrate the error caused by using the finite difference approximation.

A thermo-TDR sensor similar the one described by Wen et al. (2018) is used in this study for gradient method measurements. The thermo-TDR probe consists of three small parallel probes (1.27 mm diameter and 4.5 cm in length). Each temperature probe used in this test contains a thermistor for temperature measurement (0.46 mm diameter, 10 KΩ at 25 °C, Betatherm Inc., MA), and the heating probe is filled with a resistance wire (Ni-Cr alloy, 0.079 mm diameter, 205 Ω m^{-1}, Pelican Wire Inc., FL). Prior to the experiments, the probe spacing was calibrated using three repeated measurements in dry quartz sand with known thermal properties (Sang et al., 2021). The average value was used as the probe spacing. λ was obtained by fitting an analytical model to the DPHP temperature response curve (Liu and Si, 2008). In addition, we also used the heat flux plate HFP01 to measure G:

$$G = \frac{V_p}{E} \tag{8}$$

where V_p (mV) is the output voltage of the HFP01, and E (mV W^{-1} m^2) is the calibration constant provided by the manufacturer.

In order to compare the measurement accuracy of the heat flux plate method and the gradient method, it is necessary to have a reference G (true value) (by creating a boundary condition where the true value of the heat flux is known (Fuchs and Tanner, 1968; Howell and Tolk, 1990; Sauer et al., 2007, 2008; van Loon et al., 1998; Watts et al., 1990)). Because the steady state method is time consuming (Sauer, 2002, Pages: 1245–1246; Sauer et al., 2007, 2008; van Loon et al., 1998; Watts et al., 1990), we deployed the transient design of Fuchs and Tanner (1968) and Howell and Tolk (1990). By using a plane heater to maintain a reference G value, we designed an indoor experiment setup as shown in Fig. 1(a): a thin heating film (12 cm diameter, 0.27 mm thickness and 31.8 Ω) was placed horizontally at a depth of 5 cm in the Plexiglas container filled with soil. The heat flux plate and the thermo-TDR sensor were placed horizontally 2 cm above and below the heating film. The burial depth of both the heat flux plate (Mayocchi and Bristow, 1995; Sauer, 2002) and the DPHP probe (Heitman et al., 2008; Ochsner and Baker, 2008; Peng et al., 2017a) were similar to common field installations. A data logger (CR3000, Campbell Scientific, Inc., Logan, Utah) was used to record temperature and output voltage of the heat flux plate for 300 s at 1 s interval. The heating film divided the soil sample into two parts vertically. The heat released from the film propagated both upwards and downwards. In this way, constant heat flux boundary conditions were achieved. The heating film was connected to a DC power supply to provide a constant heating strength. The heat flux density of the heated film was set to 400 W m^{-2}.

2.3. Computer simulation

We performed COMSOL simulations to avoid the effects of various factors that impact experiments (e.g., variable wind speed (Sang et al., 2020), non-homogeneous soil structure and soil moisture distribution, vegetation (Hui et al., 2018), solar radiation fluctuations (Sang et al., 2021), non-uniform temperature field (Jury and Bellantuoni, 1976), thermal contact resistance (Liu et al., 2012) between the DPHP probe and the soil), by considering only one factor at a time. In simulations all soil physics properties, such as c, λ, α and ρ, can be defined as a function

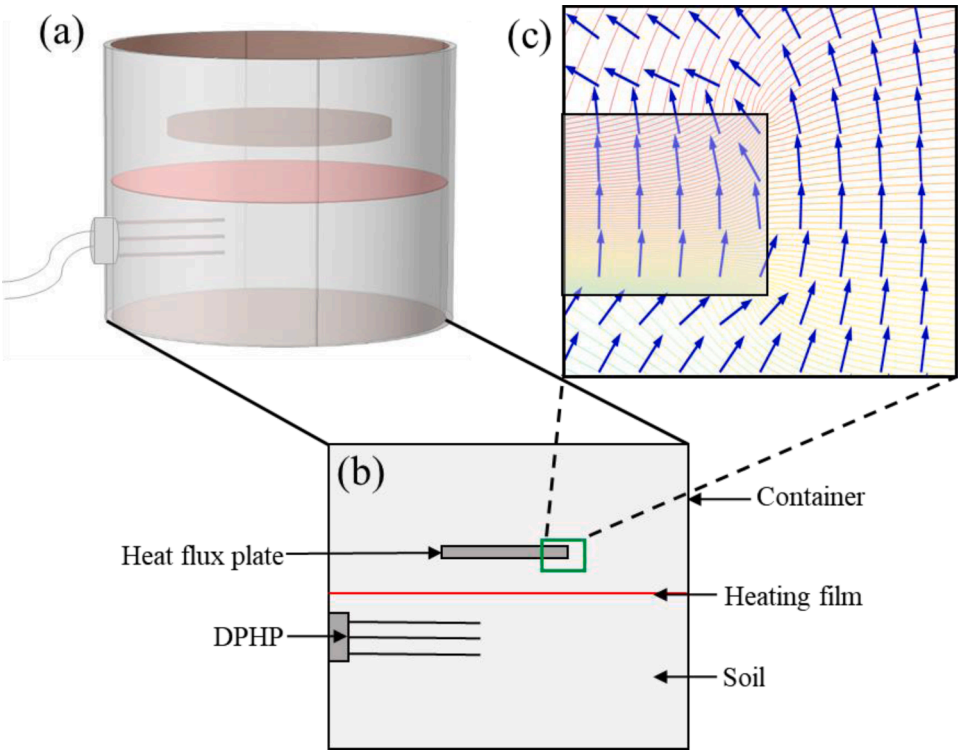

Fig. 1. (a) Schematic diagram of the indoor 3-dimensional experiment setup (not to scale); (b) The 2-dimensional cross section of Fig. 1(a) (not to scale); (c) Heat flow distortion at the end of the heat flux plate (solid lines represent isotherm curves, and arrows represent the direction of heat transfer). Here, Fig. 1(c) was the result of a 2-dimensional COMSOL simulation.

of either temperature or position. Because the COMSOL simulations provided heat flux values at selected positions without the disturbing effects of instrumentation, we can have reference values of G for comparisons. With COMSOL simulations it is possible to perform finite element calculations for materials with nonlinear material properties under complex geometrical boundaries.

Despite the advantages of computer simulations (Liu et al., 2006, 2016; Sang et al., 2020), to our knowledge, no other studies have used simulation methods to explore the sources of error in soil heat flux measurements. We used COMSOL (Version 6.0, COMSOL, Inc. Burlington, MA 01,803 USA) to simulate soil heat flux in indoor experiments (Fig. 1(a)). In the simulations, we set the vertical distance from the center of the heat flux plate to the heating film as 2 cm. Simulated temperatures at 1.4 cm, 2 cm, and 2.6 cm below the heating film were used to mimic the gradient method. The COMSOL simulations consist of five simplified processes, which are presented below:

1) Because the heat flux plate is circumferentially symmetrical, we simplify the 3D model to a 2D axisymmetric model, which greatly reduces the computational load and makes it possible to improve simulation accuracy by selecting a fine 2D mesh.
2) Compared to the model dimensions (12 cm in diameter and 10 cm high), the heating needle (1.27 mm in diameter) of the thermo-TDR/DPHP probe is simplified as a cylindrical surface heat source.
3) The thickness of the heating film (0.27 mm) is small and is approximated as a planar heat source (Fig. 1(b)).
4) We assume that the internal structure of the heat flux plate is a homogeneous medium and ignore the internal configuration and structure.
5) We ignore the convection heat transfer across the external walls of the plastic container, and set the walls as an adiabatic boundary.

In order to simulate the diurnal transient fluctuation of heat fluxes caused by solar radiation on cloudless days (Cobos and Baker, 2003; Peng et al., 2015; Sauer et al., 2007), we selected a time-varying heat flux boundary (Collares-Pereira and Rabl, 1979) at the soil-atmosphere interface

$$\frac{G_h}{G_D} = \frac{\pi}{24}(a + b\cos\omega)\frac{\cos\omega - \cos\omega_s}{\sin\omega_s - \omega_s\cos\omega_s} \tag{9}$$

where G_h (W m^{-2}) represents the hourly solar radiation and G_D (W m^{-2}) is the total daily solar radiation. ω and ω_s represent the solar angle and the sunset angle, respectively. Both a and b are functions of ω_s. We set 5:00 am as the sunrise time and 19:00 pm as the sunset time, and $G_D = 1000$ W m^{-2}. For a detailed calculation description, refer to Eq. (12) and (14) of Collares-Pereira and Rabl (1979). In order to simulate the scenario closer to our field environment (uneven soil temperature profile), we set the air-soil heat transfer coefficient at 4 W m^{-2} K^{-1} (Kosky et al., 2021; Whitaker, 1972) (an approximate 0.1 m s^{-1} breeze for our simulated soil properties) to model the existing of air convection or wind at the soil-atmosphere interface. The pre-simulated soil temperature profile at 6:00 am on the fourth day was used as the initial soil temperature profile for the final simulations.

Heat flux plates of different manufacturers have various dimensions and thermal property values (thermal conductivity λ and specific heat capacity c). As a result, plates cause various heat flow distortions (Fig. 1(c)). Four commercially available heat flux plates (Table. 2) were selected for our simulation. The filling material of these heat flux plates is epoxy resin. Because the density (ρ) and c are not provided in the product manuals, in our simulations, we kept ρ and c constant for all of the heat flux plates ($\rho = 1700$ kg m^{-3}, $c = 1300$ J kg^{-1} K^{-1}).

2.4. Field experiments

Field experiments were performed at the research station of China Agricultural University (40°1′N, 116°16′E). The experimental setup is shown in Fig. 2. To minimize the effect of heterogeneous soil texture we used the same sandy soil as in the indoor experiment. Soil was oven-dried at 105 °C and passed through a 2 mm sieve before being packed into a cylindrical container (50 cm in diameter and 20 cm deep). Similar to Sang et al. (2021), a radiometer (NR-LITE2, OTT Hydromet, Inc., Lindbergh Dr. Loveland) was used to measure incoming solar radiation (Sang et al., 2020) during the daytime. We installed the radiometer at a height of 2 cm above the soil surface to minimize the shading effect of a nearby greenhouse. In this way, the shading and the shading related temperature redistribution were reduced significantly. As a tradeoff, the solar radiation measured during the night was discarded. The 2-m elevation wind speed data were obtained from a nearby weather station. Because the HFP01SC self-calibrating heat flux plate released heat during operation (Hukseflux Thermal Sensors, 2021), it caused a disturbance in the soil temperature field (Peng et al., 2015). Therefore, for the field experiments, we used a HFP01 instead of a HFP01SC. Although typical installation depths for heat flux plates are 5 cm or deeper to avoid blocking liquid and vapor fluxes, to explore the feasibility of the DPHP method at shallow depths (less than 5 cm), a heat flux plate was buried at the same depth as the DPHP probes. Mayocchi and Bristow (1995) placed a heat flux plate at a depth of 2 cm ($z = 2$ cm). Therefore, a HFP01 was installed at $z = 2$ cm, similar to Anandakumar (1999), Mayocchi and Bristow (1995), and Sauer et al. (2007), along with a thermo-TDR probe (Wen et al., 2018). Each hour, data were collected continuously for 3 min by CR3000 (Campbell Scientific, Inc.,

Table. 2
Geometry and thermal property values of four different circular heat flux plates.

Model	Diameter m	Thickness m	Filling Material	λ W m^{-1} K^{-1}	Producer
610	0.025	0.0026	epoxy	0.33	Thornthwaite Associates, Elmer, NJ
HFP01	0.08	0.0054	epoxy	0.8	Hukseflux Thermal Sensors, Delft, the Netherlands
HFT1.1	0.038	0.0039	epoxy	1.0	Radiation and Energy Balance Systems, Seattle, WA.
HFT3.1	0.038	0.0039	epoxy	1.22	Radiation and Energy Balance Systems, Seattle, WA.

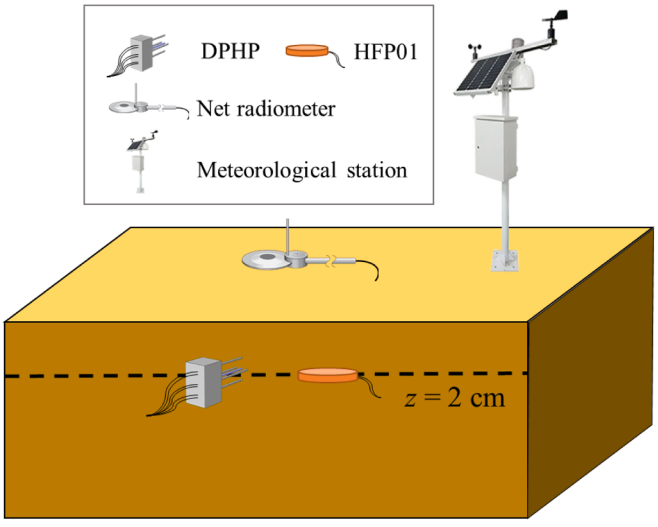

Fig. 2. Schematic diagram of the field experiment setup (not drawn to scale).

Logan, Utah) with an extension panel (AM16/32, Campbell Scientific, Inc., Logan, Utah).

2.5. Statistical analysis

To evaluate the performance of the two methods (heat flux plate and gradient method), both root mean square error (RMSE) and mean absolute error (MAE) were used,

$$RMSE = \sqrt{\frac{\sum_{i=1}^{n}(Y_i - \widehat{Y})^2}{n}} \quad (10)$$

$$MAE = \frac{1}{n}\sum_{i=1}^{n}|Y_i - \widehat{Y}| \quad (11)$$

Here Y_i and $\widehat{Y_i}$ represent the heat flux plate measured and the gradient method determined values of G, respectively. In this study, we use G_{HFP01} (the result of HFP01) as Y_i, $G_{gradient}$ (the result of gradient method) as $\widehat{Y_i}$, and n is the number of data points.

3. Results and discussion

3.1. Accuracy of COMSOL simulations

By comparing both the theoretical results of Carslaw and Jaeger (1959) (Fig. 3(a)) and the indoor experiment results (Fig. 3(b), (c)) with COMSOL simulations, we examined the feasibility of using COMSOL simulations for soil heat flux research. The accuracy of COMSOL simulations is shown in Fig. 3. For soil at two θ values (0 g g^{-1} and 0.15 g g^{-1}), $z = 2$ cm and a constant heat flux boundary $F_0 = 200$ W m^{-2}, we obtained the theoretical values of G from the analytical solution of Carslaw and Jaeger (1959, Eq. (3)). A comparison of the theoretical values with the COMSOL simulations shows that the theoretical values of G agree almost perfectly with the COMSOL finite element simulations (Pearson's correlation coefficient $r \approx 1.00$). This indicates that COMSOL simulation errors are negligible.

To further evaluate the feasibility of using COMSOL simulations, we compared the heat flux plate and gradient method measured results with the COMSOL simulation results (Fig. 3(b), (c)). The differences between the simulated results and the measured values were less than 12%. Fig. 3 (b), (c) indicates that there are some differences among the theoretical values, the measurements, and the simulations. This may be due to the deviation of the depth (distance between the heating film and the heat flux plate, and the distance between the heating film and the thermo-TDR probe) from the pre-set value ($z = 2$ cm). With an experiment, it is difficult to keep the distance or depth within an accuracy of 1 mm. In addition, the thermal contact resistance between the soil and heating film (the heat flux plate and the thermo-TDR probe as well) can also cause Eq. (3) values to be off (Sauer et al., 2007). Although the theoretical, experimental, and simulated values in Fig. 3(b), (c) do not exactly match, the three values are similar to each other, thus Fig. 3 hints that COMSOL can accurately and reliably simulate soil heat fluxes. For more general soil types beyond our research, the bulk density, heat capacity, as well as thermal conductivity are the key parameter inputs needed for the COMSOL heat conduction module.

3.2. Indoor experiments and COMSOL simulations: evaluation of two heat flux measurement methods

COMSOL simulation results are compared to the heat flux plate method and gradient method indoor experiment results. Because the soil λ values for the indoor experiments are known, we also used the Philip (1961) correction for the heat flux plate. Then we compared the measured heat flux results to the simulated values. Unlike Peng et al. (2015), who assume that the gradient method is more accurate than the heat flux plate method and use the gradient method as the reference G

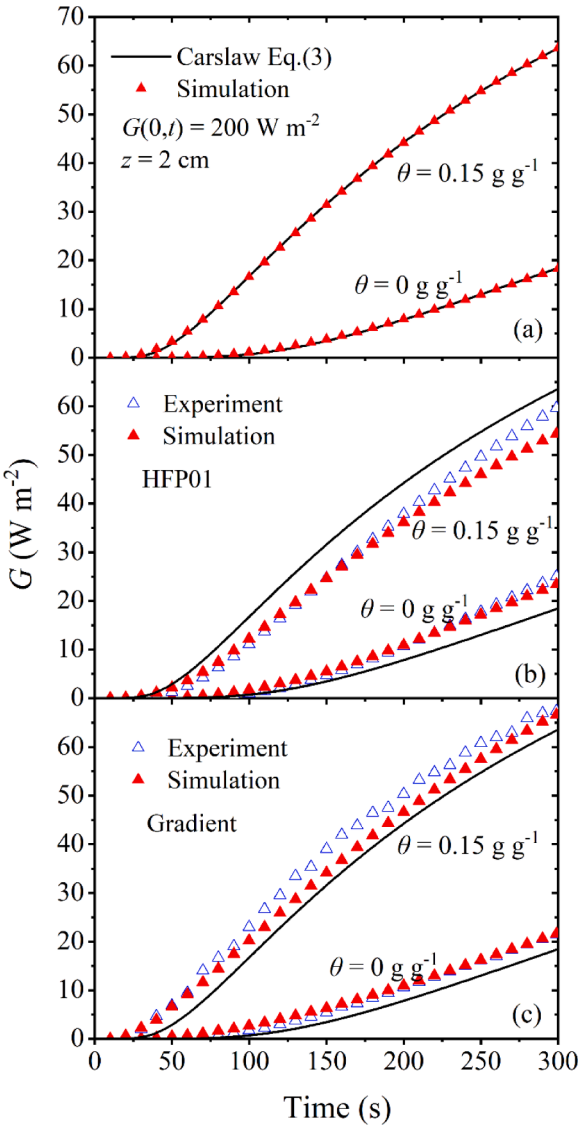

Fig. 3. (a) Comparison of G calculated by an analytical solution of Carslaw and Jaeger (1959, Eq, (3)) with G results from COMSOL simulations at two different θ values. Comparison of G measured for indoor experiments with COMSOL simulations for the heat flux plate (b) and the gradient method (c), respectively.

(true value), we perform an unbiased comparison between the gradient method and the heat flux plate method. Because, we can specify the true value of the heat flux by either using a heating film with a given heating strength, or by setting and selecting the true value in the COSMOL simulations.

The results of the indoor experiments for soil at different soil water contents θ (0 g g^{-1}, 0.02 g g^{-1} and 0.15 g g^{-1}) (Fig. 4(a), (b), (c)) show that, the heat flux plate method and the gradient method fluctuate around the theoretical value (Eq. (3)) and distribute around the 1:1 line. When $\theta = 0$ g g^{-1}, both the gradient method and the heat flux plate method overestimate the magnitude of G. Actually, the results of the gradient method are closer to the theoretical value than those of the heat flux plate. At $\theta = 0.02$ g g^{-1}, the gradient method and the heat flux plate also overestimate the magnitude of G, but the heat flux plate performs better than the gradient method. This may be due to the fact that the thermal conductivity of the heat flux plate is closer to that of the soil at this moisture content (and thus the temperature field is less distorted at the edges of the heat flux plate). For $\theta = 0.15$ g g^{-1}, the gradient method overestimates G, and the heat flux plate underestimates G. For three different θ values, the overall Pearson's correlation coefficient between

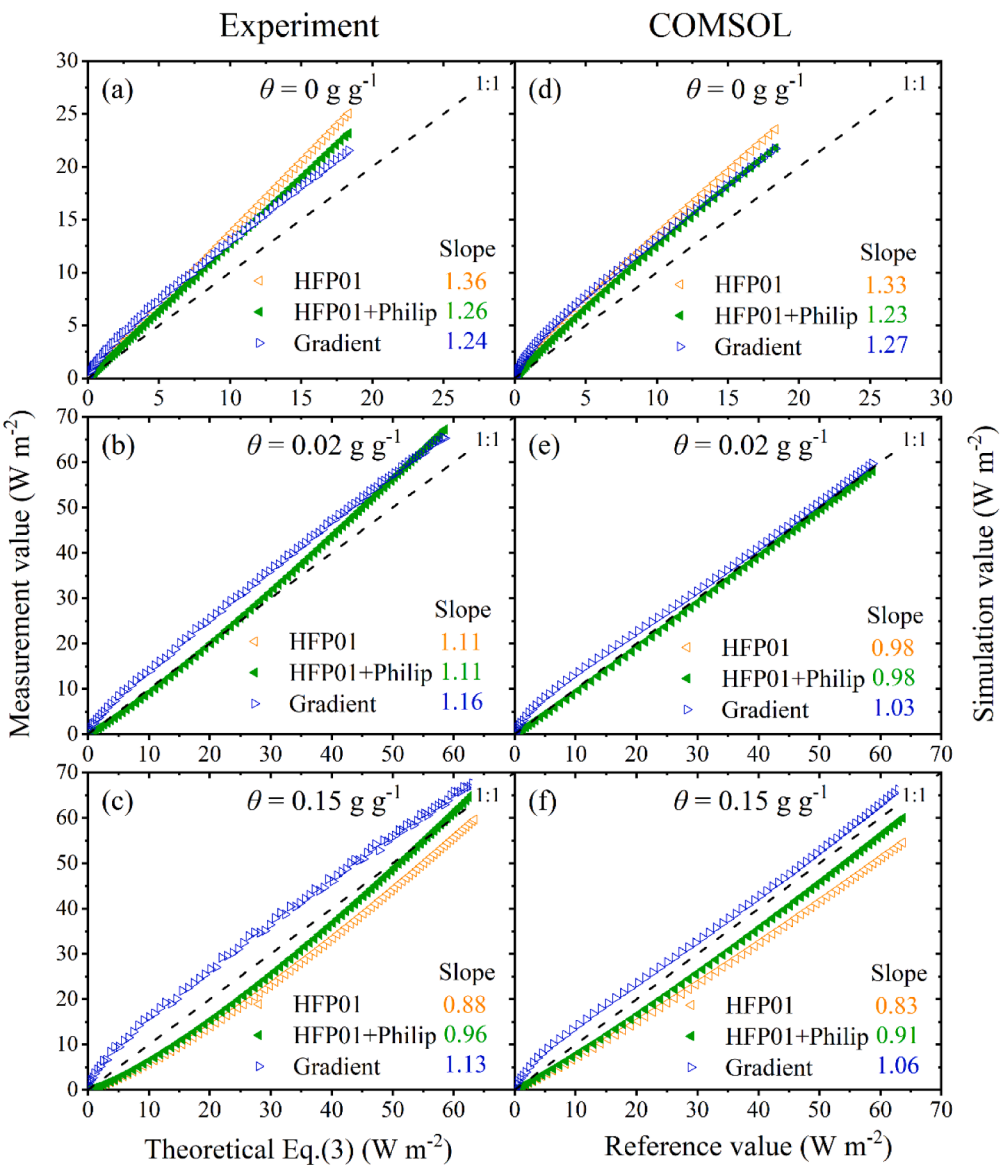

Fig. 4. Comparison of the analytical solution (Eq. (3)), gradient method and heat flux plate method for various θ values (0 g g^{-1}, 0.02 g g^{-1}, 0.15 g g^{-1}). The burial depth is z = 2 cm and the reference G (true value) of heat flux is G (0, t) = 200 W m^{-2}. (a), (b), (c) Two indoor measurements, the gradient method and the heat flux plate method are compared. Here, the analytical solution values from Eq. (3) are used as the true values for G; (d), (e), (f) Comparison of two simulations, the gradient method and the heat flux plate method. Here, the COMSOL simulated heat flux values, free from the influences of heat flux plate and DPHP probe, are used as the true values of G.

the heat flux plate method and the gradient method indicates a strong linear correlation ($r \geq 0.993$).

Fig. 4(d), (e), (f) present the COMSOL simulation results of the heat flux plate method and the gradient method for the same soil at three different θ (Fig. 3). The burial depth z and F_0 were set to be the same as the measured values. The basic trends and patterns of the COMSOL simulation results (Fig. 4(d), (e), (f)) follow the trends of the indoor experiments (Fig. 4(a), (b), (c)). At 0 g g^{-1} water content, both the gradient method and the heat flux plate overestimate the magnitude of G. The results of the gradient method are closer to the theoretical value than those of the heat flux plate. When θ = 0.02 g g^{-1}, the gradient method overestimates G and the heat flux plate underestimates it, and the results of the heat flux plate are closer to the theoretical value than the gradient method. At a moisture content of 0.15 g g^{-1}, the gradient method overestimates G and the heat flux plate underestimates it, and the gradient method is closer to the theoretical value than the heat flux plate. Fig. 4 further verifies the findings displayed in Fig. 3, i.e., the COMSOL simulations and the indoor experimental results match, and thus the COMSOL simulations can be used for probing error sources of heat flux measurements. Fig. 4 also shows that the Philip correction reduces the error of the HFP01 heat flux plate by 8% to 10% for θ = 0 g g^{-1} and 0.15 g g^{-1}. At θ = 0.02 g g^{-1}, the difference between the results before and after the Philip correction is small because the thermal conductivity of the plate is close to the soil thermal conductivity at this time which gives a correction parameter $f \approx 1$. The Philip correction formula, which can improve the measurement accuracy of the heat flux plate within a certain moisture content range, is consistent with the conclusion of Sauer et al. (2003) and Tong et al. (2019).

Because Figs. 3 and 4 illustrated the accuracy and reliability of COMSOL simulations, we used COMSOL simulations to analyze the effect of solar radiation on heat flux measurements (Fig. 5). We simulated four types of heat flux plates (Table. 2). Fig. 5 presents the simulation results for heat flux plates and for the gradient method. For ideal, clear sky conditions with the diurnal solar radiation following Eq. (9), the heat flux plate method and the gradient method can accurately measure G. Fig. 5(a) shows that 610 and HFP01 and the gradient method are close to the reference G (true value) when θ = 0 g g^{-1} (MAEs equal to 0.50 W m^{-2}, 0.91 W m^{-2}, 0.49 W m^{-2}, respectively). When θ = 0.15 g g^{-1} (Fig. 5 (b)), HFT3.1, HFP01 plates are close to the reference G with MAEs values of 0.26 W m^{-2}, 0.64 W m^{-2}, respectively, while HFT1.1 and the gradient method are less accurate with MAEs of 1.30 W m^{-2} and 1.60 W m^{-2}, respectively. In Fig. 5, the Pearson's correlation coefficient between the gradient method and the heat flux plate is $r \approx 1.00$. This indicates that the responses of both the heat flux plate and the gradient method to

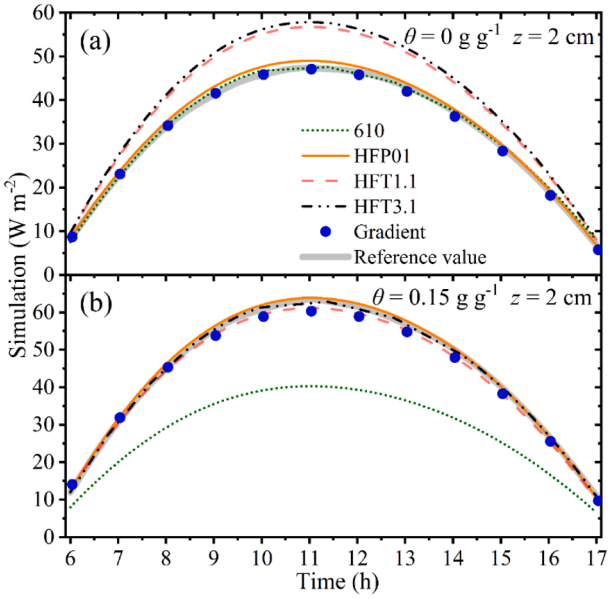

Fig. 5. COMSOL simulated G of four different heat flux plates and the G of the gradient method at θ = 0 g g^{-1} (a) and 0.15 g g^{-1} (b). Here, the temperature distribution in the soil profile is uneven and the heat flux at the soil-atmosphere interface is set to the transient periodically varying boundary conditions given by Eq. (9).

the variations of solar radiation are perfectly synchronized. Combined with the results in Figs.4 and 5, further shows that with ideal clear sky diurnal solar radiation conditions, both the heat flux plate and the gradient method provide accurate values of G.

3.3. Comparative analysis of two methods in the field and a theoretical explanation for the main gradient method error

The results in Sections 3.1 and 3.2 show that the heat flux plate and the gradient method are in good agreement with each other for measurements (or simulations) under indoor controlled conditions, and both methods can be used to obtain accurate G in barren sand. However, field conditions are more complex than controlled indoor conditions. The field temperature distribution or the soil temperature profile is not uniform (Sang et al., 2020). The soil heat flux at the soil-atmosphere interface is neither stable nor smooth, and it can randomly rise and fall. The presence of wind related convective heat transfer across the atmosphere-soil boundary (Sang et al., 2021) will violate the infinite solid assumption of both the gradient method and the DPHP method (Liu et al., 2017). In order to consider the effects of these factors on heat flux measurements, field experiments are necessary.

Field experiment results are displayed in Fig. 6. Fig. 6(a) shows the daily net radiation variation, the incoming direction of R_n gradually reverses at 8:00AM, and the heat flow changes from outflow to inflow. Between 8:00AM and 10:00AM is the time of the day when R_n rises fastest, and the peak of R_n occurs daily between 11:00AM and 13:00PM. Fig. 6(b) shows the results of the heat flux plate method and the gradient method. The peak values of G obtained by both methods also occur between 11:00AM and 13:00PM. Differences between G values

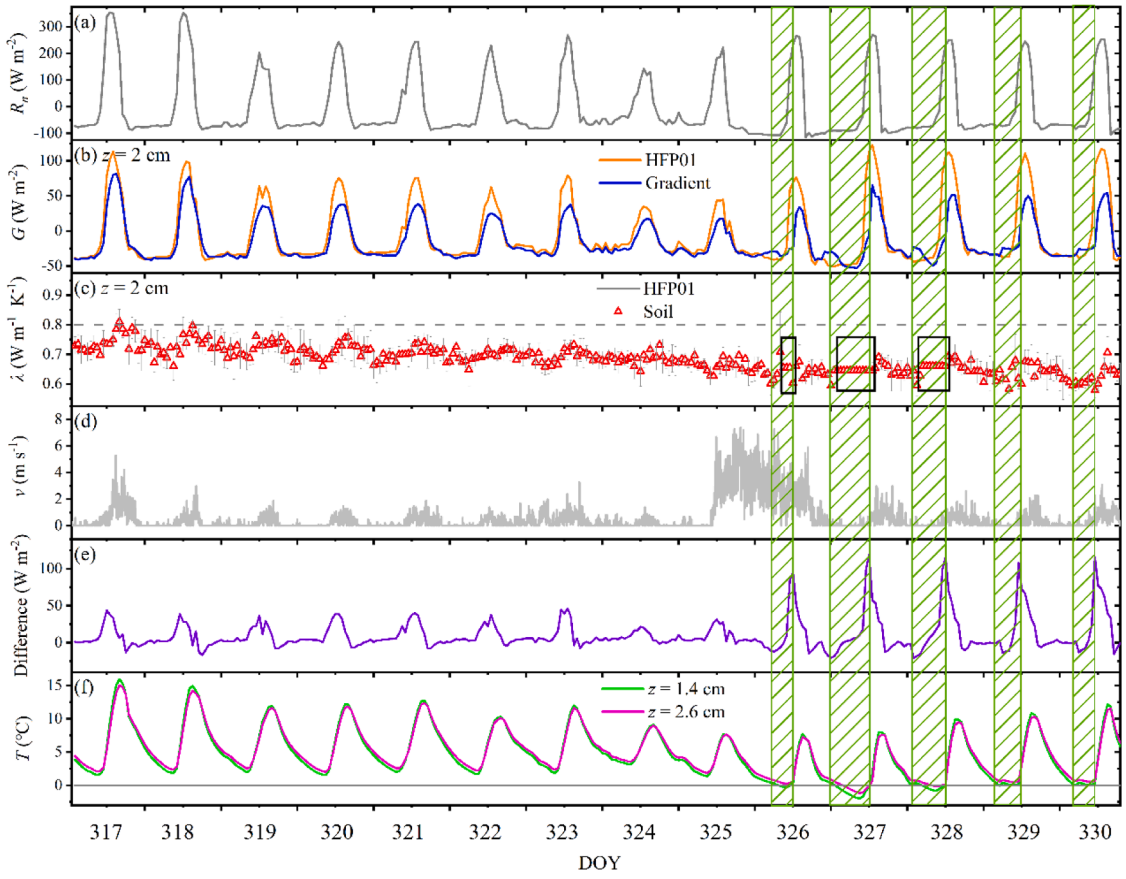

Fig. 6. Time series of field measurements (DOY317–330) of soil thermal properties and meteorological data. (a) net radiation R_n; (b) heat flux G measured at z = 2 cm; (c) hourly soil thermal conductivity (Error bars represent one standard deviation). (d) wind speed v; (e) deviation of the heat flux plate results from the gradient method results (G_{HFP01}-$G_{gradient}$); (f) soil temperature measured by two temperature probes (z = 1.4 cm and z = 2.6 cm) of the thermo-TDR probe at z = 2 cm. Green hatched areas indicate freezing periods, i.e. T < 0 °C.

measured by the two methods were between 0 and 120 W m^{-2}, which exceeded the differences in (< 30 W m^{-2}) in Fig. 5. The maximum difference occurred between 9:00AM and 11:00AM, due in part to the sensitivity of the DPHP method to radiation fluctuations and soil background temperature fluctuations (Sang et al., 2020). In this study, we used a linear background temperature de-trending method (Sang et al., 2020). Sang et al. (2021) reported that the DPHP method had the largest errors when used near noon, due in part to violations of the linear temperature trend assumption (Jury and Bellantuoni, 1976). Similar observations have also been reported by Peng et al. (2015), Sang et al. (2020), and Sang et al. (2021). The failure of the linear trend assumption may be related to solar radiation variations, background temperature fluctuations, or to transient evolution of the soil temperature profile. Because the gradient method requires accurate soil thermal conductivity values, errors in soil thermal conductivity measured by a DPHP probe will reduce the accuracy of G measured by the gradient method. As a result of the midday DPHP thermal conductivity errors, the gradient method has a larger heat flux measurement error than the heat flux plate method, especially during the midday period when the solar radiation is strong and sometimes chaotic, as can be seen in Fig. 6(c), which shows the hourly average thermal conductivity values. The increase in thermal conductivity during the midday is not due to actual physical processes, and it most likely originates from fluctuations in solar radiation and drastic changes in the soil temperature profile (Sang et al., 2020, 2021). To avoid this type of gradient method error, one should not perform midday DPHP thermal conductivity measurements. As an alternative, the early morning and evening DPHP thermal conductivity values might be used with the ambient soil temperature measurements to calculate accurate midday heat flux values. In the following section, we will provide an explanation for another potential gradient method error source and provide a theoretical way to eliminate the error.

It is well known that using a finite difference to approximate a derivative may lead to systematic errors (Thomas et al., 2014). Fig. 7 shows that all seven temperature profiles between two points (A and B) have the same finite difference value, i.e. $\Delta T/\Delta z$. However, as shown in Fig. 7(b), the errors in the derivative estimations caused by the finite difference computation are not negligible. The red line indicates the special case for temperature varying linearly with depth. In this case only, the finite difference approximation produces no error. For the other six temperature profiles, the errors in the derivative estimation may reach 50% or even 100%. It is known that the seven soil temperature profiles can occur in real field soils (Chapter 4 and Chapter 6 of Van Wijk, 1963). Therefore, using the finite difference approximation (Eq. (7)) can cause errors, especially when the temperature profile deviates from a linear function. One way to reduce the error is to reduce the value of Δz between the temperature sensing probes. The probe spacing of a DPHP sensor can be reduced, additional temperature probes can be included, or a DPHP can be placed at an angle, so the depth between the temperature probes is reduced, to minimize the error caused by using finite difference (Eq. (7)) to approximate the derivative (∇T).

The effect of reducing Δz on gradient method errors is demonstrated in Fig. 7(c): when three more temperature measurement points (i.e., locations corresponding to the gray dashed line) are added between AB, the error in the derivative calculation caused by using finite differences is significantly reduced compared to (b), and the error near point B is less than 25%. The error of the gradient method can be further reduced by adding temperature probes, i.e., reducing the value of Δz. Based on the above analysis, the error related to the gradient method is expected to be relatively large, when the soil temperature changes rapidly with depth (shallow buried probes). This is one possible explanation for the large deviations between the gradient method results and the heat flux plate results (Peng et al., 2015).

In addition to solar radiation changes causing surface temperature fluctuations, soil property variations with depth can add to temperature profile complexity (Kurylyk et al., 2015) (i.e., the soil temperature profile is not a monotonic increasing or decreasing function, but a function with local minimum or maximum). Nonuniform thermal properties and nonlinear temperature profiles decrease the accuracy of the gradient method.

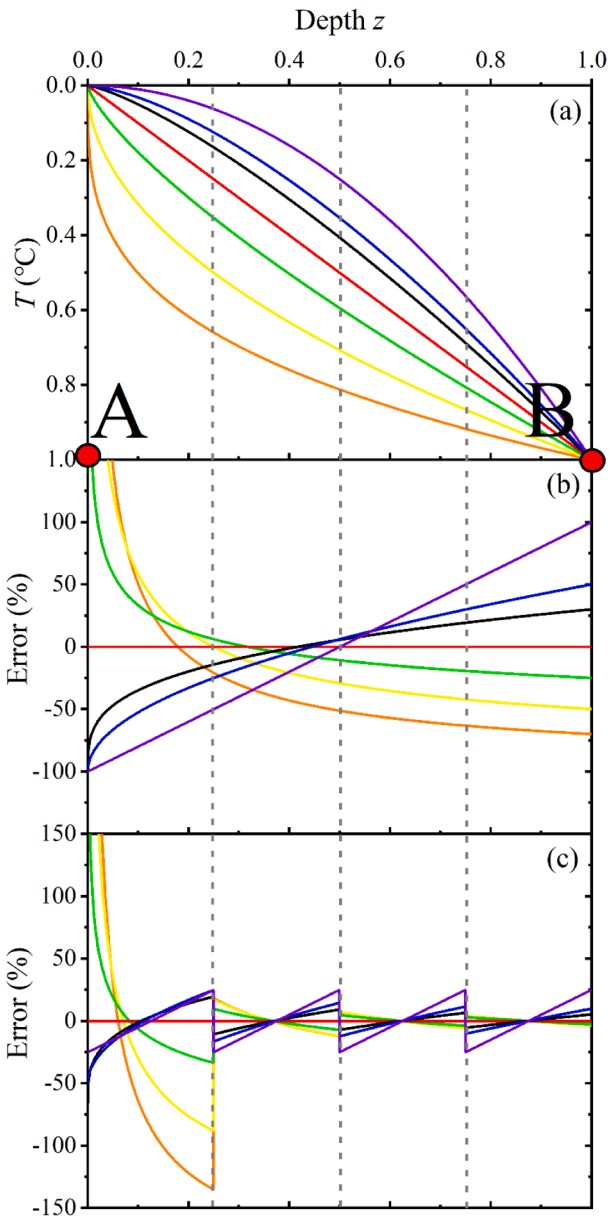

Fig 7. Illustration of the influence of soil temperature profiles (or soil temperature distribution as a function of depth) on G measurement errors of the gradient method. (a) Seven possible different soil temperature profiles between point A and point B with the red line indicating a linear temperature profile. (b) Errors with the gradient method caused by using the finite difference (Eq. (7)) to approximate the derivatives or gradients (∇T) of the soil temperature curves of (a). (c) Similar to (b) except that the temperature probe spacing Δz is 25% of (b).

Free-thaw processes can also impact heat flux measurements. The black box in Fig. 6(c) includes thermal conductivity values measured when the background temperature is near 0 °C (Fig. 6(f)). Because accurate soil thermal conductivity values are not obtained by typical DPHP probe measurements in partially frozen soils (Ochsner and Baker, 2008), gradient method heat fluxes are affected. Fig. 6(e) shows that the gradient method heat flux values deviate from the heat flux plate values during freeze-thaw periods, especially when the soil temperature is near 0 °C. Thus, there is a need to improve the DPHP method, so that it can be

used to determine accurate thermal property values and heat flux values under frozen conditions. For freeze-thaw soil conditions, we think that heat flux plate (HFP01) measurements may provide a better heat flux benchmark than gradient method values.

Fig. 6(d) shows the wind speed $v < 3.5$ m s^{-1}, except for DOY317, DOY325 and DOY326. According to Sang et al. (2020), for depths of $z >$ 16 mm, the effect of wind speed is negligible, which agrees with our soil heat flux results (Fig. 6(b)) at $z = 2$ cm.

From Fig. 8(b), (c), (d) we see that the laboratory (indoor) experiments have $R^2 > 0.98$, RMSE < 11.6 W m^{-2}, and MAE < 11.4 W m^{-2} for the two methods at three different θ values. RMSE and MAE are at their lowest when $\theta = 0$ g g^{-1}. The field results (Fig. 8(a)) are more noisy than the laboratory results ($R^2 = 0.71$ is much smaller than the laboratory result $R^2 > 0.98$), which indicates multiple sources of error in the field experiment. For example, Fig. 6(c), (e) shows that large midday radiation values and freeze-thaw soil conditions can significantly reduce the accuracy of DPHP λ values. This can cause gradient method errors to be larger in the field than in the laboratory (Fig. 8(b), (c), (d)), and sometimes larger gradient method errors than heat flux plate HFP01 errors. The field measurements had larger RMSE and MAE values than the laboratory measurements.

The correlation between the heat flux plate method and the gradient method was smaller for field conditions than for laboratory conditions (Fig. 8(b), (c), (d)). The r decreased from $r > 0.99$ to $r \approx 0.90$. Our COMSOL simulations for ideal solar radiation conditions (Fig. 5, Eq. (9)) demonstrated that there was a near perfect correlation between the heat flux plate method and the gradient method, that is $r \approx 1$. This was similar to the agreement found in the laboratory results. There was a large gap between the field and the laboratory results (and the COMSOL simulation). The solar radiation described by Eq. (9) deviated from the actual radiation (Fig. 6(a)). Eq. (9) should be used with caution to simulate G. In the future, simulations based on the actual net radiation R_n should be performed.

To clarify the sources of error in Fig. 8(a), we first compared the measurements between the heat flux plate method and the gradient method by using data collected during freeze-thaw conditions. Fig. 9 shows that for field conditions the gradient method significantly underestimates G relative to the heat flux plate method. In addition, Fig. 9 (a) also shows that the two methods are highly correlated in the absence of freeze-thaw (DOY317-DOY325) relative to the measurements during the freeze-thaw conditions (DOY326-DOY330). The corresponding Pearson's correlation coefficient r increases from 0.85 (DOY326-DOY330) to 0.97 (DOY317-DOY325), which is very close to the laboratory results ($r > 0.99$) and the results of computer simulation under ideal solar radiation conditions ($r \approx 1$). In addition, the RMSE and MAE were reduced by 58.9% and 53.5%, respectively. The freeze-thaw process corresponds to a solid-liquid phase change, and the ILS (infinite line source) model, i.e., the theoretical basis of the gradient method, does not take ice melting into account. As a result, the fitted curve of the thermo-TDR probe deviates severely from the measured temperature response values (Zhang et al., 2011). Therefore, DPHP does not accurately determine λ values during freeze-thaw conditions (Ochsner and Baker, 2008). However, when the gradient method is used to measure G, it is necessary to have accurate values of both λ (Peng et al., 2017b) and ΔT. During the field experiments from DOY326 to DOY330 the temperature at $z = 2$ cm is close to 0 °C, causing the thermo-TDR to obtain inaccurate λ values (the black boxed area in Fig. 6(c)). The limits of the DPHP method around 0 °C (Zhang et al., 2011), causes errors in the gradient method measurements of G. To avoid these errors in the gradient method, the errors associated with DPHP measurements in partially frozen soil must be reduced or eliminated. This can be done either by replacing the inaccurate λ values with reasonable λ model estimates, or, in the future, developing an improved DPHP analysis method based on introducing a moving solid-liquid interface into the existing ILS model.

Another potential error source of heat flux measurements results from variations in solar radiation. Fig. 9(b) shows that during non-freeze-thaw days (DOY317–325), that in the 09:00AM-15:00PM period the heat flux plate method and gradient method are in good agreement, relative to the 16:00PM-08:00AM time period. The slope increases from 0. 58 to close to 1 (1.06), and the RMSE and MAE

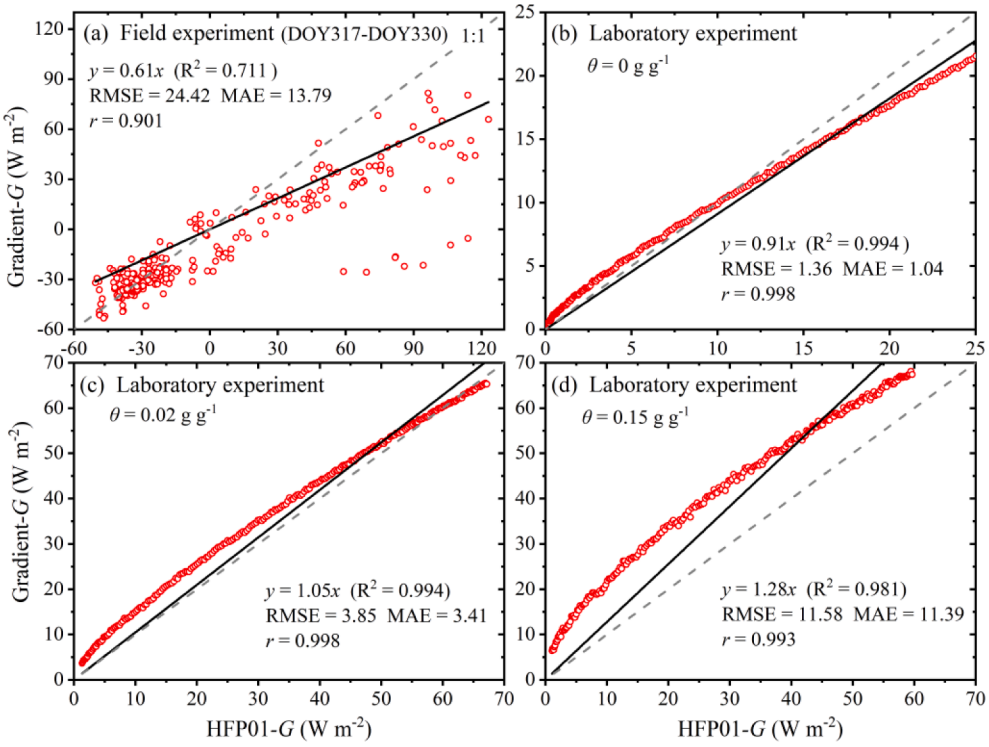

Fig. 8. Comparison of soil heat flux measurements by the heat flux plate method and the gradient method ($z = 2$ cm). (a) Results of field G measurements (DOY317-DOY330); (b) (c) (d) Indoor G measurements at different moisture contents (0 g g^{-1}, 0.02 g g^{-1}, 0.15 g g^{-1}). (Note, the units of both RMSE and MAE are W m^{-2}.).

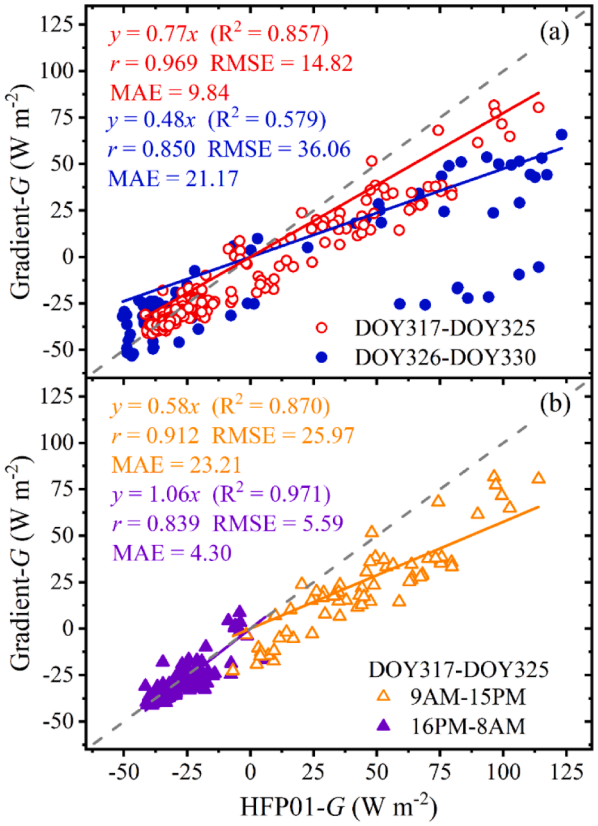

Fig. 9. Correlations between heat flux plate measurements and gradient method measurements at $z = 2$ cm for the field experiments. (a) G measurements including freeze-thaw conditions (DOY326-DOY330) and without freeze-thaw conditions (DOY317-DOY325); (b) G measurements at two different daily time periods (09:00AM-15:00PM and 16:00PM-08:00AM) during DOY317-DOY325. (Note: r denotes Pearson's correlation coefficient; the units of both RMSE and MAE are W m^{-2}.).

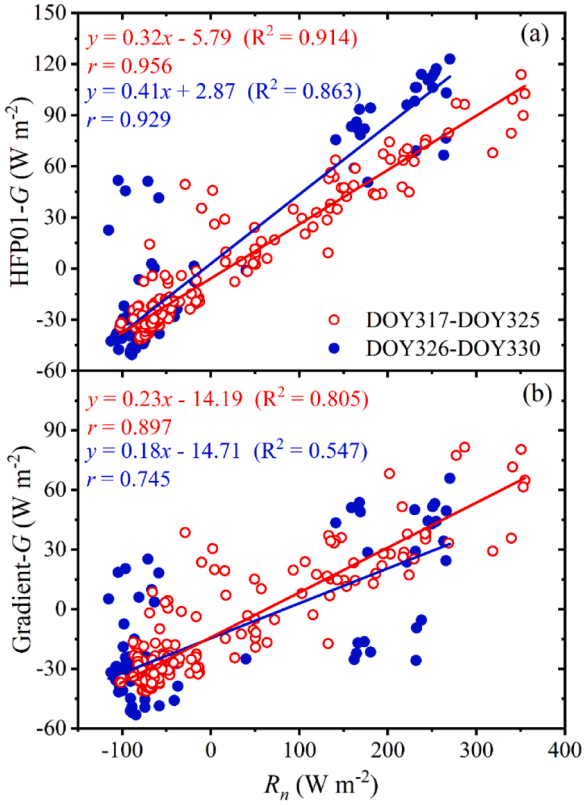

Fig. 10. Correlation analyses of net radiation R_n with (a) HPF01 values of field heat flux and (b) gradient method values of field heat flux. (Note: r denotes Pearson's correlation coefficient).

decrease by 78.5% and 81.5%, respectively. Each day the period from 09:00AM to 15:00PM has relatively high wind speeds (Fig. 6(d)), implying that wind influences the results. Under field conditions, surface soils undergo periodic heating and cooling in response to daily variations in solar radiation. Our experiments (Fig. 6(e)) show that the daily absolute error between the heat flux plate and the gradient method has a regular pattern: the maximum relative errors occur coincidently with the daily G peak (9:00AM to 15:00PM). Solar radiation heats the soil surface, and warmer soil can promote air circulation, which can lead to an increase in surface air flow. Wind can effect the transient evolution of the soil temperature profile, causing a non-linear background temperature trend to develop, Which leads to errors in soil thermal property determination (Sang et al., 2020, 2021). In addition, a varying surface temperature is more likely to cause the soil temperature profiles to deviate from the linear profile assumed by the gradient method (Eq. (5)), which can also lead to systematic errors in the application of the finite difference approximation to the thermal gradient term in Fourier's law. A similar conclusion by Gao et al. (2017) supports our deduction. They found that G is sensitive to changes in soil thermal conductivity and soil thermal diffusivity during daytime measurements. To our knowledge, no other study (Ochsner et al., 2006; Peng et al., 2015; 2017b) included an error analysis on, the effects of wind or air convection on heat flux G determinations based on DPHP measurements. The effects of wind or air convection need further clarification by performing high resolution soil temperature profile measurements.

In the absence of freeze-thaw (DOY317-DOY325), R_n is strongly correlated with the HFP01 measured G, with Pearson's correlation coefficient $r = 0.96$ (Fig. 10(a)). Even though the gradient method uses the erroneous midday λ values, the r value is quite large at 0.90 (Fig. 10(b)). The r values would be even larger if the early morning and evening λ values are used during the midday period. During freeze-thaw conditions, r decreases for both methods, however, for the heat flux plate method r decreases by only 2.8%, while, for the gradient method, r decreases by 16.9%. Thus, the freeze-thaw process significantly reduces the measurement accuracy of the gradient method, which is consistent with the results presented in Fig. 9(a).

Based on COMSOL simulations using ideal solar radiation conditions (Eq. (9)), correlation coefficient r values were determined for R_n and G for both the gradient method and the heat flux plate method. The results show that $r > 0.97$ for both the flux plate method and the gradient method. This hints that under ideal solar radiation conditions given by Eq. (9), the heat flux plate and gradient methods perform similarly. In practice, heat flux plates are buried 5 cm or deeper to avoid distorting soil water content profiles due to disruptions of liquid and vapor fluxes. So, heat flux plates and DPHP gradient methods both have strengths and weaknesses. Our results indicate that heat flux plates are preferred during freeze-thaw conditions. When using DPHP sensors for gradient method determinations, the early morning or evening λ values should be used for calculations. In addition, by reducing the number of heating periods per day, we can minimize heat distortions from DPHP sensors.

Precipitation did not occur during the field study, water infiltration was negligible. Thus, water infiltration and its effects on heat flux plate measurements were not considered in this experiment. There are other potential sources of errors for heat flux plates, such as the contact thermal resistance between the plate and soil particles (Sauer et al., 2007), and changes in soil bulk density (Ochsner et al. (2006); Peng et al. (2017b)). All of these issues can be further studied in the future.

4. Conclusions

There exists a need for an effective method to compare and assess the measurement errors and performance of the heat flux plate method and the gradient method. In this study, the performances of the two heat flux measurement methods are compared and analyzed through laboratory (indoor) experiments, field (outdoor) experiments, and computer simulations. For laboratory experiments, we controlled the soil heat flux by using a heating film with a given heating strength. The laboratory correlation coefficients between the heat flux plate method and the gradient method G measurements are $r > 0.99$. However, the field measurements had r of 0.90. The DPHP-based gradient method is not able to determine G accurately during freezing and thawing soil conditions, because the DPHP method does not determine λ of partially frozen soil accurately. In order for the DPHP-based gradient method to perform well as during the midday when the solar radiation is strong and more chaotic, the early morning or evening λ values should be used. We recommend the use of a heat flux plate to measure G under freeze-thaw conditions. As to the gradient method, we demonstrated that increasing the spatial resolution of temperature measurement by reducing probe spacing Δz can improve the accuracy of this method to measure G. The laboratory measured values are similar to the COMSOL simulation results (relative deviation $< 12\%$), which indicates that the G simulations are reliable. Future soil heat flux measurements should be evaluated for a range of soil types and vegetations.

Declaration of Competing Interest

The authors declare that they have no known competing financial interests or personal relationships that could have appeared to influence the work reported in this paper.

Data availability

The data that has been used is confidential.

Acknowledgements

This work was supported by the Natural Science Foundation of China (Grant No. 42077008 and Grant No. 41771257), the US National Science Foundation (Grant No. 2037504) and USDA-NIFA Multi-State Project 4188.

References

Anandakumar, K., 1999. A study on the partition of net radiation into heat fluxes on a dry asphalt surface. Atmos. Environ. 33, 3911–3918. https://doi.org/10.1016/S1352-2310(99)00133-8.

Carslaw, H.S., Jaeger, J.C., 1959. Conduction of Heat in Solids, 2nd Edition. Oxford University Press, New York.

Choudhury, B.J., Idso, S.B., Reginato, R.J.J.A., 1987. Analysis of an empirical model for soil heat flux under a growing wheat crop for estimating evaporation by an infrared-temperature based energy balance equation. Agric. For. Meteorol. 39, 283–297. https://doi.org/10.1016/0168-1923(87)90021-9.

Cobos, D.R., Baker, J.M., 2003. In situ measurement of soil heat flux with the gradient method. Vadose Zone J. 2, 589–594. https://doi.org/10.2136/vzj2003.5890.

Collares-Pereira, M., Rabl, A., 1979. The average distribution of solar radiation-correlations between diffuse and hemispherical and between daily and hourly insolation values. Sol. Energy 22, 155–164. https://doi.org/10.1016/0038-092X(79)90100-2.

Faucher-Giguère, C.-A., Lidz, A., Hernquist, L., 2008. Numerical simulations unravel the cosmic web. Science 319, 52–55. https://doi.org/10.1126/science.1151476.

Foken, T., Dlugi, R., Kramm, G., 1995. On the determination of dry deposition and emission of gaseous compounds at the biosphere-atmosphere interface. Meteorol. Z. 4, 91–118. https://doi.org/10.1127/METZ/4/1995/91.

Foken, T., 2008. The energy balance closure problem: an overview. Ecol. Appl. 18, 1351–1367. https://doi.org/10.1890/06-0922.1.

Fuchs, M., Tanner, C.B., 1968. Calibration and Field Test of Soil Heat Flux Plates 32, 326–328. https://doi.org/10.2136/sssaj1968.03615995003200030021x.

Gao, Z.M., Russell, E.S., Missik, J.E.C., Huang, M.Y., Chen, X.Y., Strickland, C.E., Clayton, R., Arntzen, E., Ma, Y.L., Liu, H.P., 2017. A novel approach to evaluate soil heat flux calculation: an analytical review of nine methods. J. Geophy. Res. Atmos. 122, 6934–6949. https://doi.org/10.1002/2017jd027160.

Heitman, J.L., Horton, R., Sauer, T.J., Desutter, T.M., 2008. Sensible heat observations reveal soil-water evaporation dynamics. J. Hydrometeorol. 9, 165–171. https://doi.org/10.1175/2007jhm963.1.

Howell, T.A., Tolk, J.A., 1990. Calibration of Soil Heat Flux Transducers. Theor. Appl. Climatol. 42, 263–272. https://doi.org/10.1007/bf00865987.

Hui, F., Zhu, J., Hu, P., Meng, L., Zhu, B., Guo, Y., Li, B., Ma, Y., 2018. Image-based dynamic quantification and high-accuracy 3D evaluation of canopy structure of plant populations. Ann. Bot. 121, 1079–1088. https://doi.org/10.1093/aob/mcy016.

Hukseflux Thermal Sensors B.V. HFP01SC self-calibrating heat flux sensor user manual. https://www.hukseflux.com/products/heat-flux-sensors/heat-flux-meters/hfp01sc-heat-flux-sensor, 2021.

Idso, S.B., Aase, J.K., Jackson, R.D., 1975. Net radiation — Soil heat flux relations as influenced by soil water content variations. Boundary Layer Meteorol. 9, 113–122. https://doi.org/10.1007/BF00232257.

Jury, W.A., Bellantuoni, B. 1976. A background temperature correction for thermal conductivity probes. 40, 608–610. 10.2136/sssaj1976.03615995004000040040x.

Kimball, B.A., Jackson, R.D., Nakayama, F.S., Idso, S.B., Reginato, R.J., 1976. Soil-heat flux determination: temperature gradient method with computed thermal conductivities. Soil Sci. Soc. Am. J. 40, 25–28. https://doi.org/10.2136/sssaj1976.03615995004000010011x.

Kosky, P., Balmer, R., Keat, W., Wise, G., 2021. Chapter 14 - Mechanical Engineering. In: Kosky, P., Balmer, R., Keat, W., Wise, G. (Eds.), Exploring Engineering, Fifth Edition. Academic Press, pp. 317–340. https://doi.org/10.1016/B978-0-12-815073-3.00014-4.

Kurylyk, B., Macquarrie, K., Caissie, D., McKenzie, J., 2015. Shallow groundwater thermal sensitivity to climate change and land cover disturbances: derivation of analytical expressions and implications for stream temperature modeling. Hydrol. Earth Syst. Sci. 19, 2469–2489. https://doi.org/10.5194/hess-19-2469-2015.

Leuning, R., van Gorsel, E., Massman, W.J., Isaac, P.R., 2012. Reflections on the surface energy imbalance problem. Agric. For. Meteorol. 156, 65–74. https://doi.org/10.1016/j.agrformet.2011.12.002.

Liu, G., Si, B.C., 2008. Dual-probe heat pulse method for snow density and thermal properties measurement. Geophys. Res. Lett. 35, 5. https://doi.org/10.1029/2008gl034897.

Liu, G., Li, B.G., Hu, K.L., van Genuchten, M.T., 2006. Simulating the gas diffusion coefficient in macropore network images: influence of soil pore morphology. Soil Sci. Soc. Am. J. 70, 1252–1261. https://doi.org/10.2136/sssaj2005.0199.

Liu, G., Li, B.G., Ren, T.S., Horton, R., Si, B.C., 2008. Analytical solution of heat pulse method in a parallelepiped sample space with inclined needles. Soil Sci. Soc. Am. J. 72, 1208–1216. https://doi.org/10.2136/sssaj2007.0260.

Liu, G., Si, B.C., Jiang, A.X., Li, B.G., Ren, T.S., Hu, K.L., 2012. Probe body and thermal contact conductivity affect error of heat pulse method based on infinite line source approximation. Soil Sci. Soc. Am. J. 76, 370–374. https://doi.org/10.2136/sssaj2011.0228n.

Liu, G., Zhao, L.J., Wen, M.M., Chang, X.P., Hu, K.L., 2013. An adiabatic boundary condition solution for improved accuracy of heat-pulse measurement analysis near the soil-atmosphere interface. Soil Sci. Soc. Am. J. 77, 422–426. https://doi.org/10.2136/sssaj2012.0187n.

Liu, G., Wen, M.M., Ren, R.Q., Si, B.C., Horton, R., Hu, K.L., 2016. A general in situ probe spacing correction method for dual probe heat pulse sensor. Agric. For. Meteorol. 226, 50–56. https://doi.org/10.1016/j.agrformet.2016.05.011.

Liu, G., Lu, Y.L., Wen, M.M., Ren, T.S., Horton, R., 2017. Advances in the heat-pulse technique: improvements in measuring soil thermal properties. Methods Soil Anal. 2. https://doi.org/10.1002/saj2.20148.

Lu, S., Ma, C.M., Meng, P., Zhang, J.S., Zhang, X., Lu, Y.L., Yin, C.J., 2016. Experimental investigation of subsurface soil water evaporation on soil heat flux plate measurement. Appl. Therm. Eng. 93, 433–437. https://doi.org/10.1016/j.applthermaleng.2015.09.058.

Mauder, M., Foken, T., Cuxart, J., 2020. Surface-energy-balance closure over land: a review. Boundary Layer Meteorol. 177, 395–426. https://doi.org/10.1007/s10546-020-00529-6.

Mayocchi, C.L., Bristow, K.L., 1995. Soil surface heat flux: some general questions and comments on measurements. Agric. For. Meteorol. 75, 43–50. https://doi.org/10.1016/0168-1923(94)02198-S.

Ochsner, T.E., Baker, J.M. 2008. In Situ Monitoring of Soil Thermal Properties and Heat Flux during Freezing and Thawing. 72, 1025–1032. 10.2136/sssaj2007.0283.

Ochsner, T.E., Sauer, T.J., Horton, R., 2006. Field tests of the soil heat flux plate method and some alternatives. Agron. J. 98, 1005–1014. https://doi.org/10.2134/agronj2005.0249.

Peng, X.Y., Heitman, J., Horton, R., Ren, T.S., 2015. Field evaluation and improvement of the plate method for measuring soil heat flux density. Agric. For. Meteorol. 214, 341–349. https://doi.org/10.1016/j.agrformet.2015.09.001.

Peng, X.Y., Wang, Y., Heitman, J., Ochsner, T., Horton, R., Ren, T.S., 2017a. Measurement of soil-surface heat flux with a multi-needle heat-pulse probe. Eur. J. Soil Sci. 68, 336–344. https://doi.org/10.1111/ejss.12421.

Peng, X.Y., Heitman, J., Horton, R., Ren, T.S., 2017b. Determining near-surface soil heat flux density using the gradient method: a thermal conductivity model-based approach. J. Hydrometeorol. 18, 2285–2295. https://doi.org/10.1175/jhm-D-16-0290.1.

Philip, J.R., 1961. The theory of heat flux meters. J. Geophys. Res. 66, 571–579.

Ren, T.S., Noborio, K., Horton, R., 1999. Measuring soil water content, electrical conductivity, and thermal properties with a thermo-time domain reflectometry

probe. Soil Sci. Soc. Am. J. 63, 450–457. https://doi.org/10.2136/sssaj1999.03615995006300030005x.

Russell, E., Liu, H., Gao, Z., Finn, D., Lamb, B., 2015. Impacts of soil heat flux calculation methods on the surface energy balance closure. Agric. For. Meteorol. 214, 189–200. https://doi.org/10.1016/j.agrformet.2015.08.255.

Sang, Y.J., Liu, G., Horton, R., 2020. Wind effects on soil thermal properties measured by the dual-probe heat pulse method. Soil Sci. Soc. Am. J. 84, 414–424. https://doi.org/10.1002/saj2.20041.

Sang, Y.J., Liu, G., Ren, T.S., 2021. Field test of two background temperature correction methods of dual probe heat pulse method. Geoderma 401, 115349. https://doi.org/10.1016/j.geoderma.2021.115349.

Sauer, T.J., Meek, D.W., Ochsner, T.E., Harris, A.R., Horton, R., 2003. Errors in heat flux measurement by flux plates of contrasting design and thermal conductivity. Vadose Zone J. 2, 580–588. https://doi.org/10.2136/vzj2003.5800.

Sauer, T.J., Ochsner, T.E., Horton, R., 2007. Soil heat flux plates: heat flow distortion and thermal contact resistance. Agron. J. 99, 304–310. https://doi.org/10.2134/agronj2005.0038s.

Sauer, T.J., Ochsner, T.E., Heitman, J.L., Horton, R., Moorman, T.B. 2008. Careful measurements and energy balance closure – the case of soil heat flux.

Sauer, T.J., 2002. Heat flux density. In: Topp, G.C., Dane, J.H. (Eds.), *Methods of Soil Analysis. Part 4. Physical Methods*. SSSA Book Series no. 5. Soil Science Society of America, Madison, Wisconsin, pp. 1233–1248. https://doi.org/10.2136/sssabookser5.4.c52.

Thomas, George, B., Weir, Maurice, Hass, Joel, 2014. Thomas' Calculus, 14th edition. Pearson Press.

Tong, B., Sauer, T.J., Gao, Z.Q., Xiao, X.H., Horton, R., 2019. Improving soil heat flux accuracy with the Philip correction technique. J. Hydrometeorol. 20, 1435–1448. https://doi.org/10.1175/jhm-D-18-0243.1.

van Loon, W.K.P., Bastings, H.M.H., Moors, E.J., 1998. Calibration of soil heat flux sensors. Agric. For. Meteorol. 92, 1–8. https://doi.org/10.1016/s0168-1923(98)00090-2.

Van Wijk, W.R., 1963. Physics of Plant Environment. North-Holland Publishing Co, Amsterdam.

Watts, D.B., Kanemasu, E.T., Tanner, C.B., 1990. Modified heat-meter method for determining soil heat flux. Agric. For. Meteorol. 49, 311–330. https://doi.org/10.1016/0168-1923(90)90004-p.

Wen, M.M., Liu, G., Horton, R., Lu, Y.L., Ren, T.S. 2018. Summary of Advances in the Heat-Pulse Technique: improvements in Measuring Soil Thermal Properties. 82, 1016-1016. 10.2136/sssaj2018.02.0067.

Whitaker, S., 1972. Forced convection heat transfer correlations for flow in pipes, past flat plates, single cylinders, single spheres, and for flow in packed beds and tube bundles. AlChE J. 18 (2), 361–371. https://doi.org/10.1002/aic.690180219.

Wilson, K., Goldstein, A., Falge, E., Aubinet, M., Baldocchi, D., Berbigier, P., Bernhofer, C., Ceulemans, R., Dolman, H., Field, C., Grelle, A., Ibrom, A., Law, B.E., Kowalski, A., Meyers, T., Moncrieff, J., Monson, R., Oechel, W., Tenhunen, J., Valentini, R., Verma, S., 2002. Energy balance closure at FLUXNET sites. Agric. For. Meteorol. 113, 223–243. https://doi.org/10.1016/s0168-1923(02)00109-0.

Wu, B.Q., Oncley, S.P., Yuan, H.L., Chen, F., 2020. Ground heat flux determination based on near-surface soil hydro- thermodynamics. J. Hydrol. (Amst) 591, 125578. https://doi.org/10.1016/j.jhydrol.2020.125578.

Zhang, Y., Treberg, M., Carey, S.K., 2011. Evaluation of the heat pulse probe method for determining frozen soil moisture content. Water Resour. Res. 47, W05544. https://doi.org/10.1029/2010WR010085.